RGNZ/MGPB

Low Frequency Passive Seismic Analysis for Characterizing Hydrocarbon Presence in the Kendal Subbasin

Maman Rohaman[1]* ✉, **Alfathony Krisnabudhi**[2] ✉, **Hasan Tri Atmojo**[2] ✉, **Ikhwannur Adha**[2] ✉

[1] *Geophysical Engineering, Universitas Pembangunan Nasional Veteran Yogyakarta, Padjadjaran Street, Sleman Regency, Yogyakarta Special Region, Indonesia.*

[2] *Geological Engineering, Universitas Pembangunan Nasional Veteran Yogyakarta, Padjadjaran Street, Sleman Regency, Yogyakarta Special Region, Indonesia.*

Abstract

This study explores the characteristics of hydrocarbon presence in the Kendal subbasin, Central Java, using low-frequency passive seismic (LFPS) techniques as a direct hydrocarbon indicator. Waveform data were collected in 2024 using five deployed stations, including areas near oil wells, oil seeps, and non-seepage zones, to assess the presence of hydrocarbons trapped within fault-bounded anticlines. The thrust faults in the study area significantly influence the Kerek Formation, creating structural folds that serve as potential hydrocarbon traps. In analysing that potential trap system, the waveform data is processed following the time windowing and bandpass filtering to enhance signal clarity and isolate relevant seismic responses. This study identified significant Power Spectral Density (PSD) anomalies within the 1-4 Hz frequency range, which aligns with anomalies observed in Vertical-to-Horizontal Spectral Ratio (VHSR) data. The consistent occurrence of these anomalies in both PSD and VHSR data highlights the potential of LFPS as a reliable tool for detecting subsurface hydrocarbons in geologically complex regions like the Kendal subbasin. The polarity analysis was also performed, resulting in an average azimuth of 0.43° NNE, with an average dip of 0.68°. These results inform us that the hydrocarbon flows from the border fault in the north to the well. This method complements the other geophysical method analysis to find new hydrocarbon opportunities.

1. Introduction

The research focuses on the Kendal region in Central Java Province, aiming to investigate the presence of hydrocarbons through geophysical data analysis. **Sribudiyani et al.** (**2003**) developed maps depicting the basement and basin types during the 35-20 Ma period. These maps indicate that the Kendal subbasin is located north of the volcanic arc and associated with the continental crust. The subbasin is part of a back-arc basin, bordered by the Waleri High, which divides the Kendal and Pemalang subbasins in the west. In the east, a basement high separates the Kendal subbasin from the Muria Trough extension in the Semarang area.

Figure 1 depicts the basin configuration from 20-5 Ma, highlighting basement and surface structures. In Central Java, the primary basement structural trend is oriented at 109°N. However, the rose diagram reveals minor structural trends in the NW-SE direction, indicat-ing localized structural patterns within the study area. Confirming that statement, **Jamal et al**. (**2024**) analysed the geological structure of the Kendal area using Near-Infrared (NIR) and Shortwave Infrared: the main structure of this area is a thrust fault with E-W trend; the NW-SE structural trend with strike-slip fault mechanism that intersects the main thrust fault; and the other NE-SW strike-slip fault trend that was formed after the thrust fault.

The confirmed presence of hydrocarbons makes this area particularly significant in a geoscience context. Several locations within the subbasin are established as hydrocarbon-producing zones. The NCJA and Cipluk/Klantung wells have successfully yielded hydrocarbons (**Audithia et al., 2016**), and oil seeps have also been discovered in various parts of the region, suggesting further hydrocarbon potential.

Low-frequency passive seismic (LFPS) is a method often applied as a direct hydrocarbon indicator (DHI). **Saenger et al. (2009)** conducted the low-frequency passive seismic survey in the Burgos basin, Northeastern Mexico, focusing on tight gas reservoirs. They acquired low-frequency passive seismic data in the 1-6 Hz range.

---

* Corresponding author: Maman Rohaman

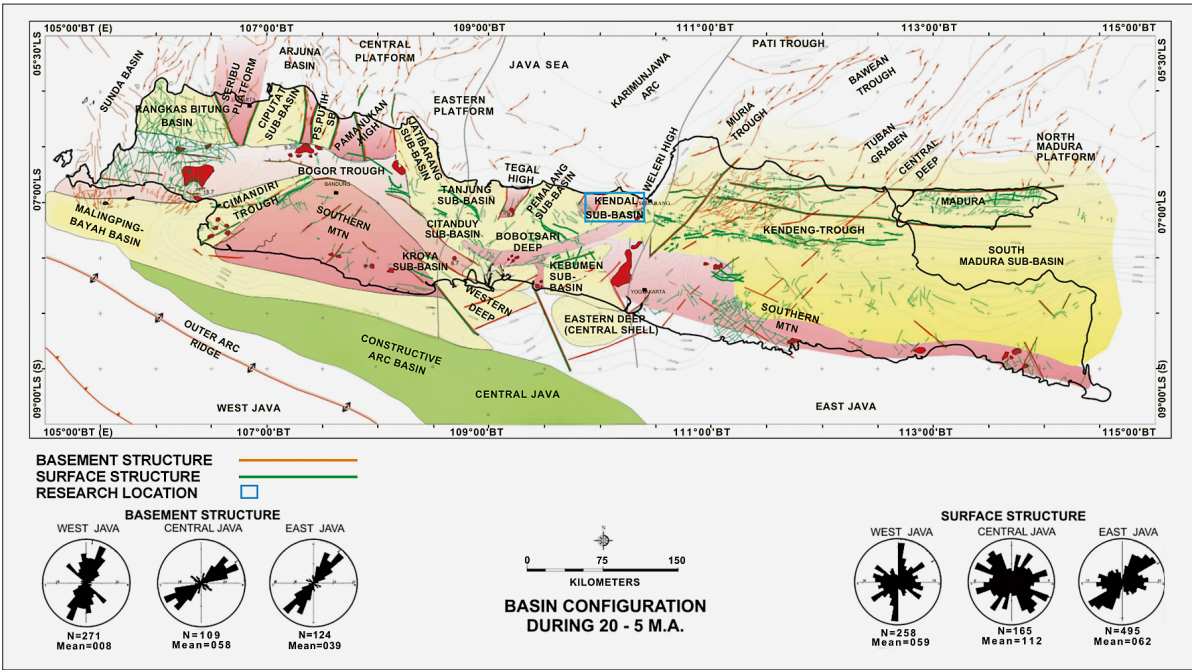*e-mail address: maman.rohaman@upnyk.ac.id*

Figure 1. Basin Configuration of Java Island during 20-5 Ma (**Sribudiyani et al., 2003**)

Their findings suggest that poroelastic effects caused by wave-induced fluid movements and oscillations of different fluid phases are detectable in the low-frequency spectrum. The study indicates that the hydrocarbons in the reservoir are partially or, in some areas, fully saturated, revealing important insights into reservoir conditions.

Priyono et al. (2023) analysed the Banyubang oil field using LFPS. Priyono et al. collected and examined data, identifying prospective zones validated by results from proven locations. Their study found that the anomalies detected were not always vertically polarized, and these anomalies could intensify daily, necessitating calibration for accurate interpretation.

As noted by **Audithia et al. (2016)**, the study area is where many wells have been abandoned. In this study, three wells were used to analyse the LFPS response. These wells are still releasing oil mined traditionally by the local community. In addition to the sounding locations, one oil seepage location also wants to analyse the LFPS response. In addition, there is one location that will be used as a blind test. The location is still within the same continuity structure as these wells. LFPS analysis starts with data selection and filtering, Power Spectral Density (PSD) of vertical components, and Vertical-to-Horizontal Spectral Ratios (VHSR).

1.1. Regional stratigraphy

The geological study of the Kendal region provides insights into the stratigraphic framework and tectonic events that shaped the subsurface layers (see **Figure 2**). Key formations identified in the study area and structural features like intrusions help to build a comprehensive understanding of the region's geological history.

Figure 2. Stratigraphic column of the Kendeng Zone (after **Thanden et al., 1996**)

1.1.1. Basement

Although the basement rocks are not exposed in the study area, previous work by **Adha (2021)** indicates that the basement lies at depths ranging from 4500 to 6000 meters. According to **Koulakov et al. (2007)**, in a depth slice of 5 km, the p-wave velocity in this area ranges from 5.01 to 5.43 km/s. This velocity value is too high for the Paleogene sedimentary rock. In other words, the results illustrate that the basement depth estimation is shallower than 5 km.

1.1.2. Pelang Formation

The Pelang Formation, described by **Sukardi and Budhitrisna (1992)**, is composed primarily of marl with
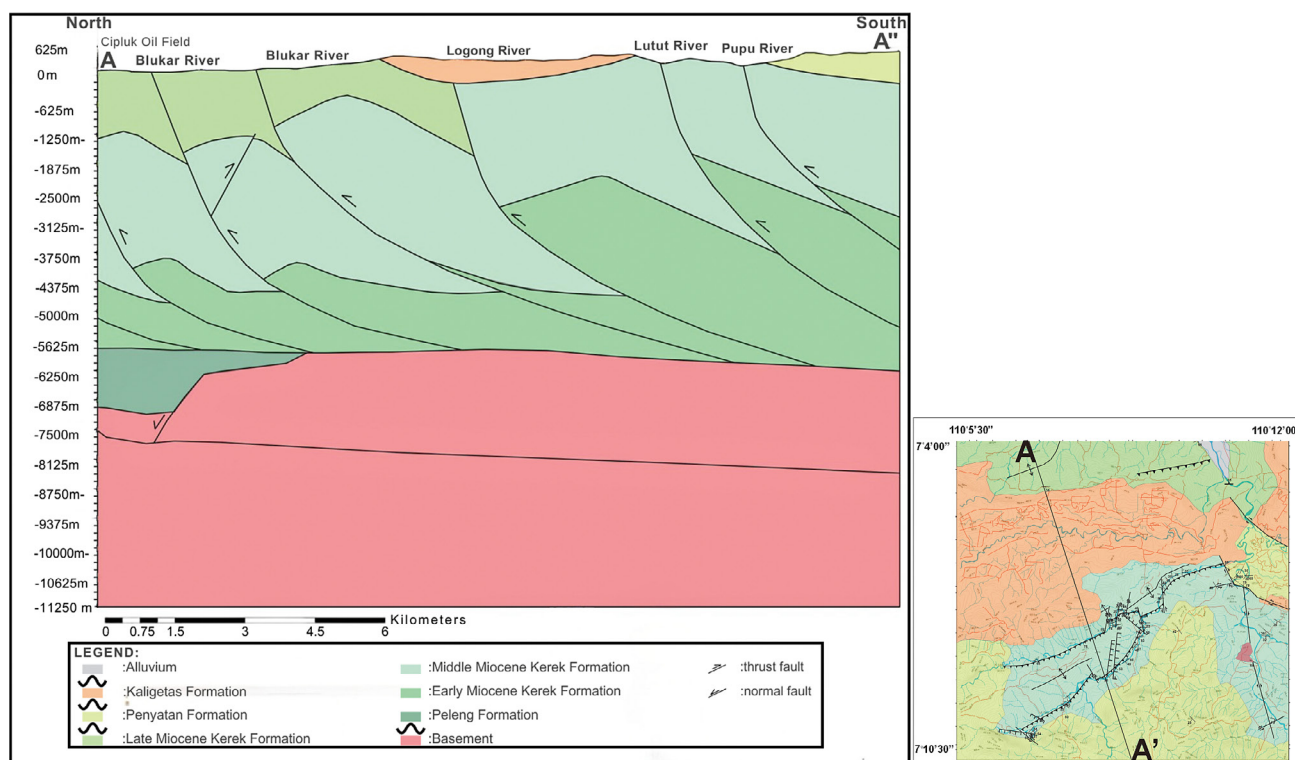
Figure 3. The structural style of the Kerek Formation that has oil and gas trap potential (after **Adha, 2019**)

limestone intercalations. It was deposited in a deep-sea environment from the Oligocene to the Late Miocene, predating the Kerek Formation.

1.1.3. Kerek Formation

The Kerek Formation consists of mudstone interbedded with limestone or sandstone, as noted by **Adha** (**2019**) and **Nurhandoko et al.** (**2020**). It can be divided into three members based on their geological age: Early, Middle, and Late Miocene. The Middle Miocene Kerek Formation consists predominantly of mudstone and sandstone, with limestone at the base and sandstone at the top, reflecting deposition in a slope morphology within an upper bathyal environment. The Late Miocene Kerek Formation is dominated by thick mudstone with limestone intercalations deposited in upper to middle bathyal environments.

1.1.4. Andesite Intrusion

An andesite intrusion penetrates the Kerek Formation, forming a sill-type structure. This intrusion is estimated to have occurred during the Pliocene after the Kerek Formation had formed and undergone deformation.

1.1.5. Penyatan Formation

The Penyatan Formation is characterized by sandstone with intercalations of mudstone and breccia in specific locations. In some areas, sandstone also contains mudstone intercalations. This formation was deposited in a bathyal environment during the Pliocene.

1.1.6. Kaligetas Formation

The Kaligetas Formation is primarily composed of breccia, with occasional sandstone layers. This formation represents volcanic material deposits from the Pliocene to Pleistocene, highlighting significant volcanic activity during this period.

1.1.7. Damar Formation

The Damar Formation consists predominantly of tuffaceous sandstone and breccia. Like the Kaligetas Formation, it was deposited during the Pliocene to Pleistocene, indicating continued volcanic activity and sedimentation in the region.

1.1.8. Alluvium

The alluvial unit represents more recent deposits formed from river processes in the study area. It consists of a mixture of rock fragments, including sandstone, limestone, and igneous rocks, with sizes ranging from boulders to silt. This unit reflects ongoing erosional and depositional processes shaping the landscape in modern times.

1.2. Regional structural geology

The geological structures in the study area, as classified by **Adha and Sapiie** (**2019**), can be divided into three main groups: normal faults, thrust faults with folds, and strike-slip faults. The potential reservoir in this area is Kerek, which has a geological age of Early to Late Miocene.
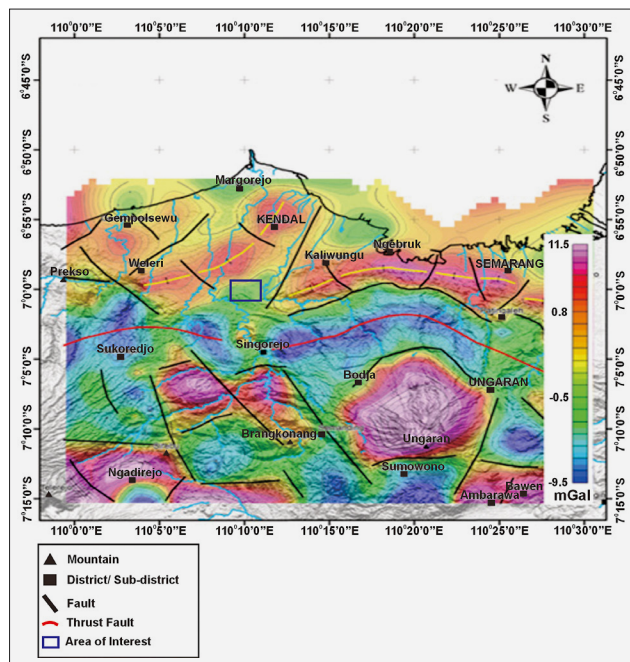
Figure 4. Completed Bouguer Anomaly (CBA) in the research area (**Jamal et al, 2024**)

1.2.1. Normal Faults

Though the normal fault group is not directly exposed in the study area, its existence is inferred based on its west-east trend. These faults are associated with basin development that provided space for the deposition of the Pelang Formation.

1.2.2. Thrust Faults and Folds

The thrust fault and fold system trends southwest-northeast and dips toward the southeast. These faults primarily affect the Kerek Formation, where they form folds

and act as potential traps for hydrocarbons, indicating their significance in oil and gas exploration (see **Figure 3**).

1.2.3. Strike-Slip Faults

A north-south orientation characterizes the strike-slip fault group and represents a dextral (right-lateral) movement. This fault system is considered the last major deformation event in the study area, occurring during the Pliocene to Pleistocene epochs. The recent structure configuration is illustrated by CBA in **Figure 4**. The Kendal subbasin is located in the marked box, showing the area of interest.

2. Methods

2.1. Data acquisition

In 2024, low-frequency passive seismic data was acquired with point spacing between 190 - 330 meters. **Figure 5** shows the station location for data acquisition. The data collection spanned two days, with each station being measured for 1 hour. The waveform data was saved in mseed format with a sampling rate of 1 second. The waveform was recorded in the three-component seismometer, vertical, east-west (E-W), and north-south (N-S) direction. Station 1, Station 3 and Station 4 are located near well locations that emit oil. Station 2 is positioned along a riverbank where oil seepage was observed, originating from fractured, exposed rock formations. Station 5, located on the same structural trend, shows no visible oil seepage. The remaining locations were near non-producing wells, although oil was still leaking from these sites.

2.2. Data processing

Figure 6 illustrates the methodological workflow of the study. The process initiates with a geological assess-
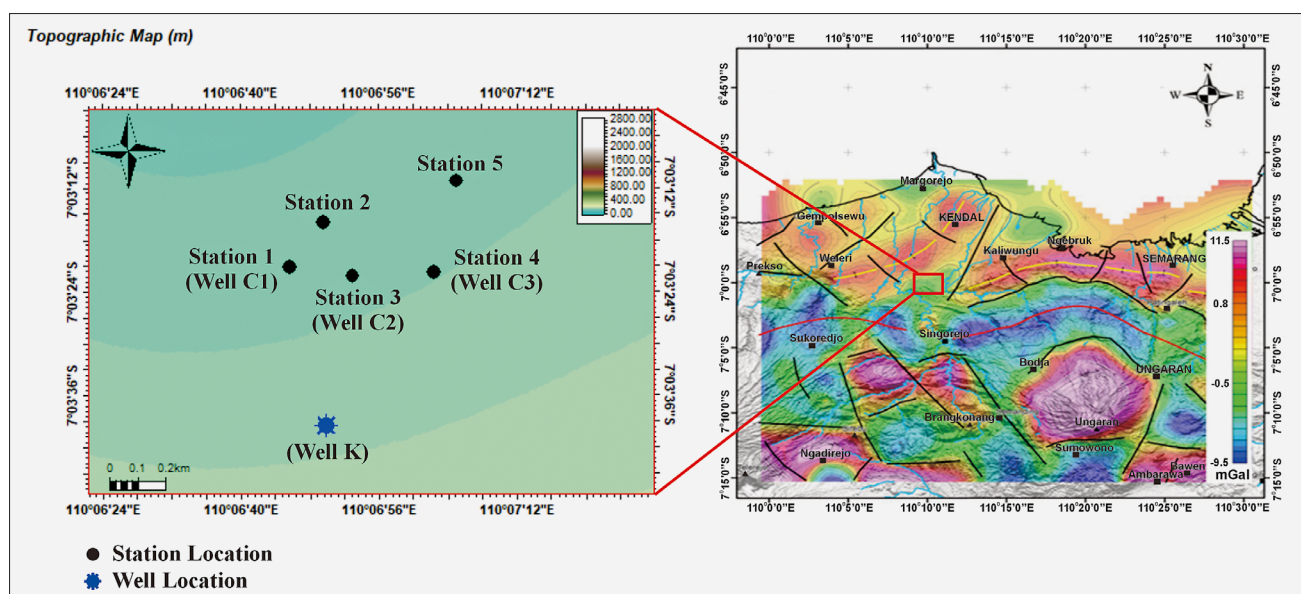

Figure 5. Low-frequency passive seismic data acquisition using a Three-Component Seismometer
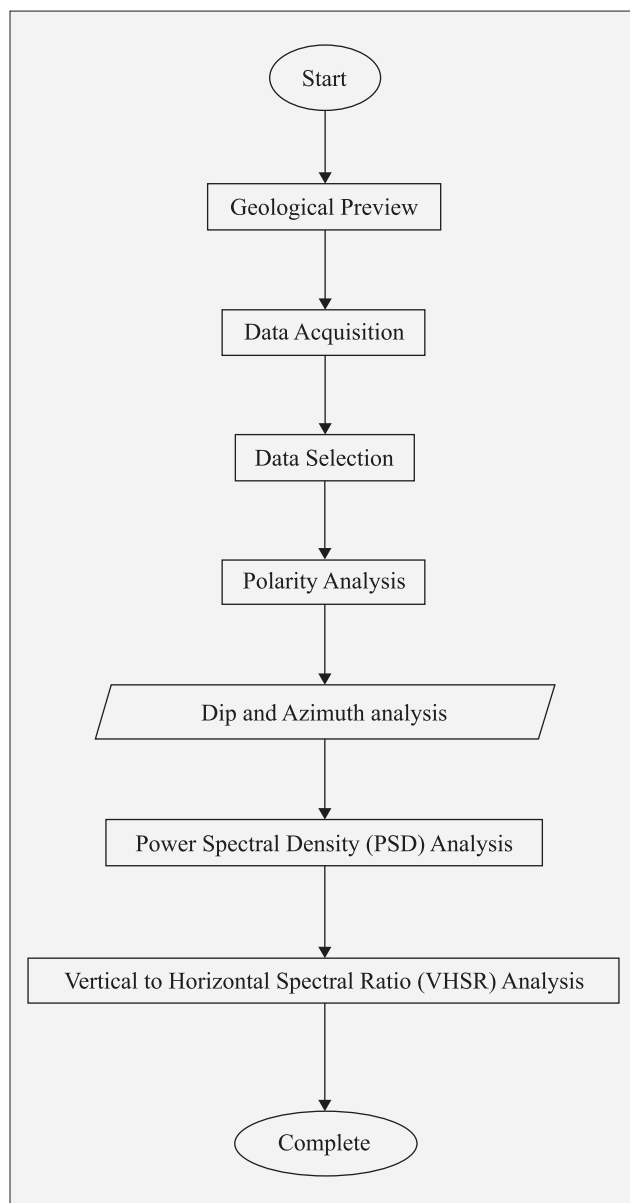
Figure 6. Workflow chart

ment to guide the design of the data acquisition strategy. Data acquisition is then executed, primarily focusing on regions with confirmed hydrocarbon occurrences. The subsequent steps in data processing include selecting relevant data, applying filters, conducting polarization analysis, performing Power Spectral Density (PSD) analysis, and evaluating the Vertical-to-Horizontal Spectral Ratio (VHSR).

2.1.1. Data Selection

The waveform data collected at each site consisted of 3600 individual data sample. To facilitate data selection, the ground motion response was plotted. **Figure 7** displays the ground motion response (top) and the frequency spectrum (bottom). **Yang et al. (2020)** highlighted that the time-frequency diagram provides a more intuitive way to observe both the arrival time and frequency components of seismic waves, offering enhanced clarity in seismic data analysis. Therefore, by analysing the frequency spectrum, data with high-frequency content will be filtered out and excluded from subsequent processing steps.

2.1.2. Data Filtering

The subsequent stage involves data filtering. During this phase, the selected data undergo trend removal and frequency filtering using a zero-phase bandpass filter (**Saenger, 2009**). Several references utilize low-frequency filters. **Haris et al. (2019)** utilized a frequency range of 0.2-6 Hz. **Priono et al. (2023)** utilized its frequency range of 0.2-6 Hz. This study employs a filter frequency range of 0.1 to 10 Hz. This filter design is still relevant to highlight the LFPS. This process eliminates any residual high-frequency components that may have persisted after the initial manual data selection. **Figure 7** shows the consistency of data selection assisted by this data filtering. The reduction of data that has high-frequency content helps the data selection to focus more on low-frequency microtremor data.
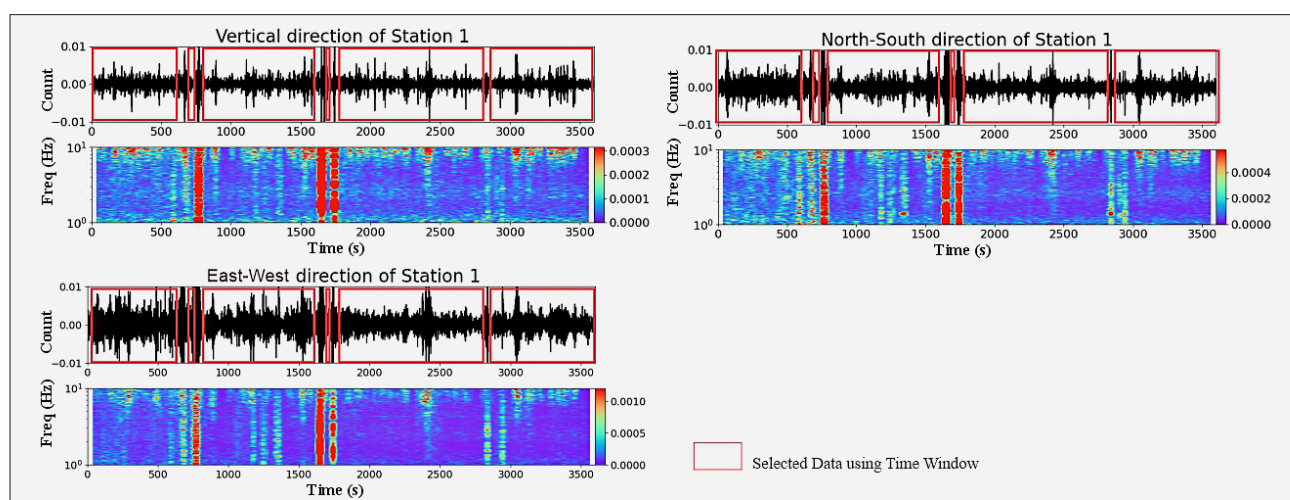

Figure 7. Three-Component of ground motion and its frequency spectrum recorded by Station 1
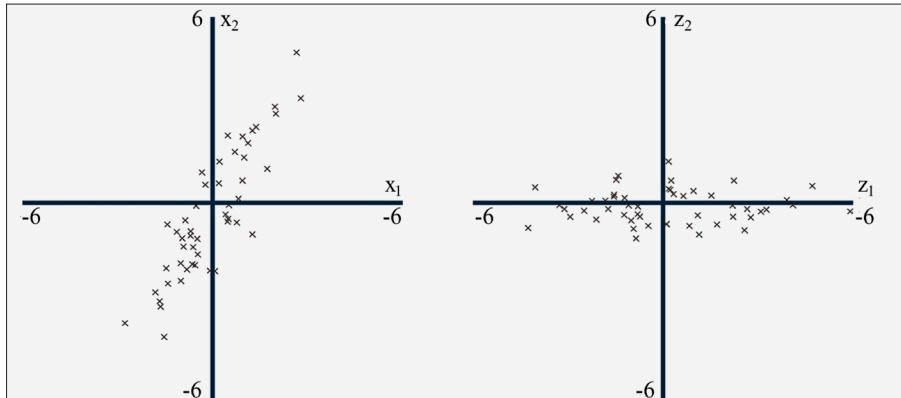
Figure 8. Crossplot of 50 observations for the variables x_1 and x_2 on the left side. Crossplot after transforming them into their corresponding principal components, z_1 and z_2 (**Jolliffe, 2002**).
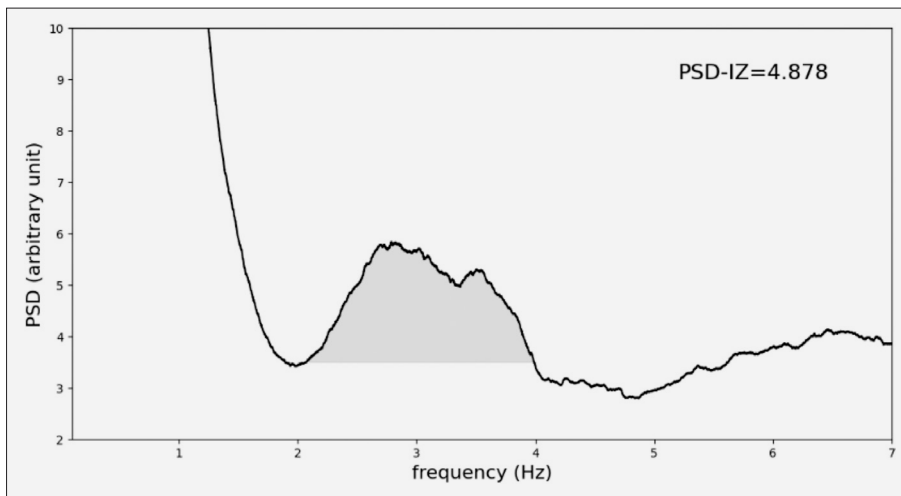

Figure 9. A power spectral density anomaly is detected in low-frequency

2.1.3. Polarization

Polarization analysis is used to obtain the resultant response from the three-component waveform data, which can represent the direction of seismic waves induced by fluid movement. Dip and Azimut are the end products of polarization analysis. However, before obtaining these two parameters, the waveform data must first be analysed to obtain eigenvectors using PCA.

Generally, Principal Component Analysis (PCA) is the method utilized for feature delineation. PCA transforms the original set of m variables into new variables, known as components, which are linear combinations of the initial variables (**Davis, 2006; Flood et al., 2015**). This transformation is performed such that each new component captures a portion of the dataset's total variance, with successive components accounting for decreasing amounts of variance (**Flood et al., 2015; Rohaman, 2022**). In **Figure 8**, two variables are depicted on a 2D plane and converted into two principal components. This transformation allows for better classification of the observed data along the component axes.

PCA generates the orientation of the new component relative to the original component. It shows the dominant contribution of three-component waveform data illustrated by the largest eigenvector (p_1). Using that re-

sult, dip φ and azimuth θ can be calculated by following **Equation 1** and **2** below:

$$\varphi = \tan^{-1} \frac{p_1(V)\sqrt{2}}{\sqrt{p_1(H_{EW})^2 + p_1(H_{NS})^2}} \quad (1)$$

$$\theta = \tan^{-1} \frac{p_1(H_{NS})}{p_1(H_{EW})} \quad (2)$$

Respectively, V, H_{NS}, and H_{EW} are vertical component, north-south component and east-west component.

The dip angle (φ) is defined as 0° for horizontal polarization and increases to 90° as it aligns with the positive vertical axis. The azimuth angle (θ) is measured anticlockwise from the north.

2.1.4. Power Spectral Density (PSD)

The next step involves analysing the filtered waveform data through the vertical component. Since the dataset is in a time series format, it is transformed into the frequency domain for further analysis. Within this domain, peak amplitudes in the vertical component are identified in the 1-4 Hz frequency range and then integrated to produce the Power Spectral Density (PSD) (**Priyono et al., 2023**). PSD-IZ is a calculation of the
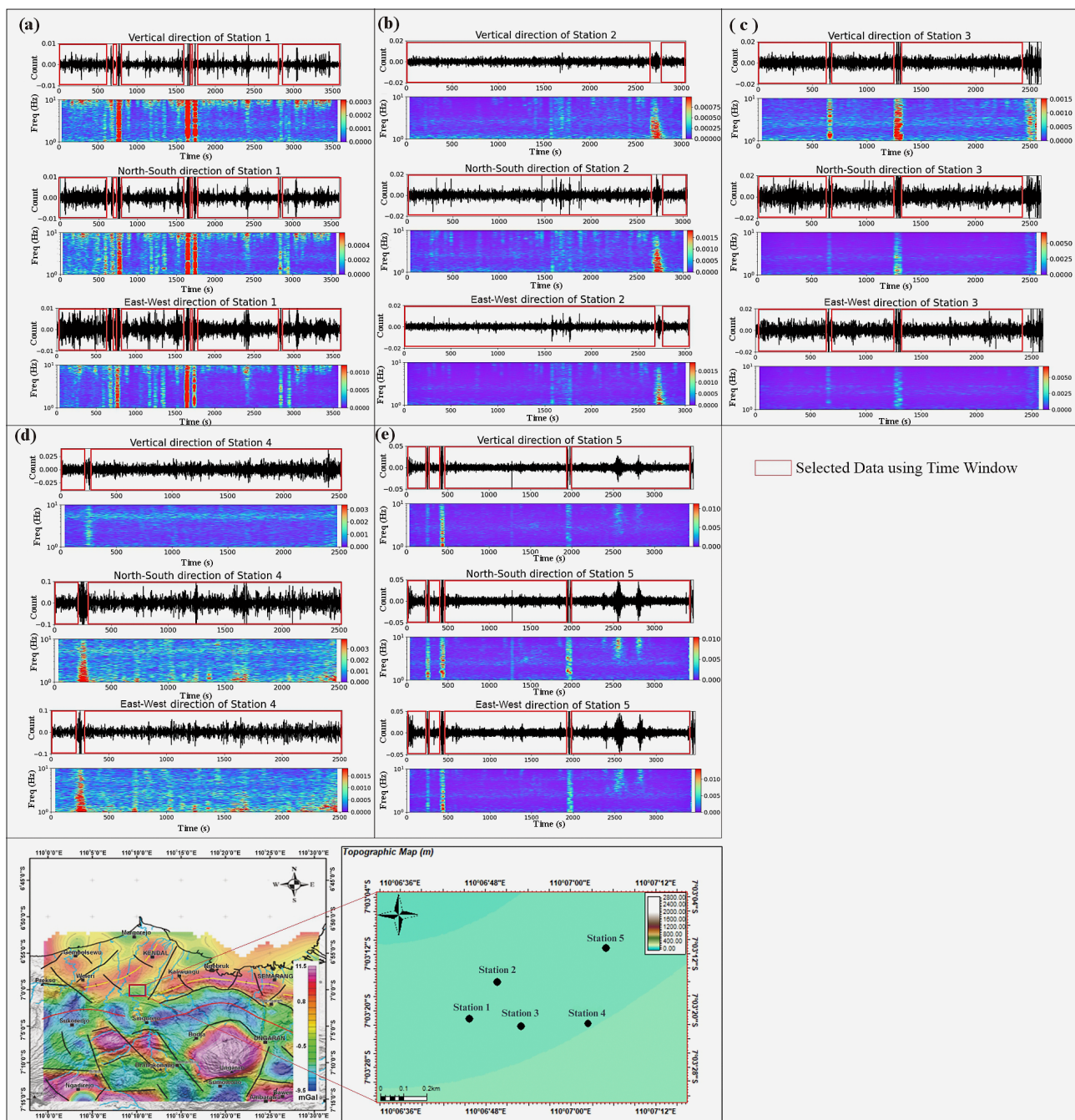
Figure 10. Three-component ground motion and its spectrum for data selection and filtering for (a) Station 1, (b) Station 2, (c) Station 3, (d) Station 4 and (e) Station 5.

PSD anomaly area at a low-frequency range. Priyono et al. calculated the PSD-IZ at the station deployed around the well. The value range of PSD-IZ is 4.3-27.2. **Saenger et al. (2009)** also performed such calculations. The PSD-IZ calculation results for the low producer well are around 150-500. At the same time, the PSD-IZ in other producer wells is around 500-5000. **Figure 9** displays the PSD derived from the vertical component.

2.1.5. VHSR

Lambert et al., and Saenger et al., introduced an approach for quantifying spectral anomalies related to hy-

drocarbons known as the Vertical-to-Horizontal Spectral Ratio (VHSR) method (**Lambert et al., 2009; Saenger et al., 2009**). This technique operates on the principle that seismic waves propagating from beneath the surface will resonate with the receiver, leading to dominance in the vertical component's amplitude. The horizontal component's spectral amplitude is determined using the **Equation 3** provided below:

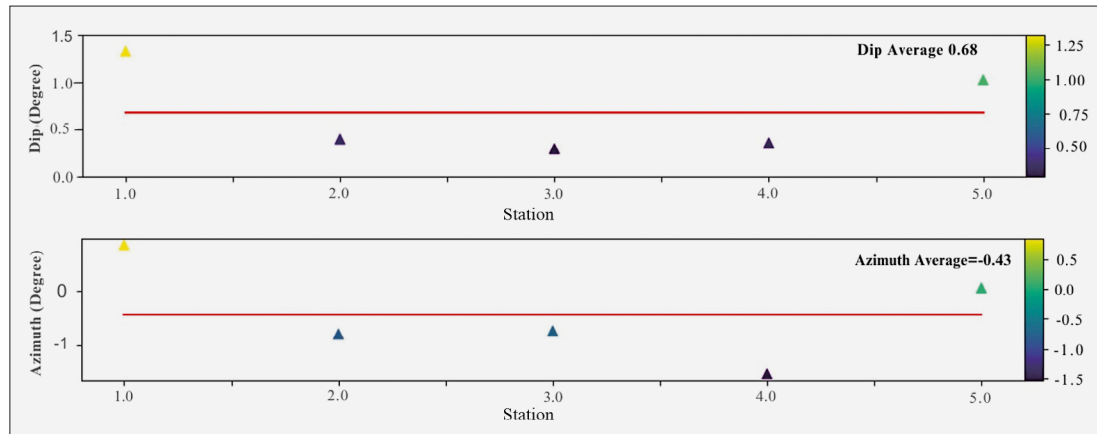$$H(f) = \sqrt{\frac{H_{EW}^{2} + H_{NS}^{2}}{2}} \qquad (3)$$

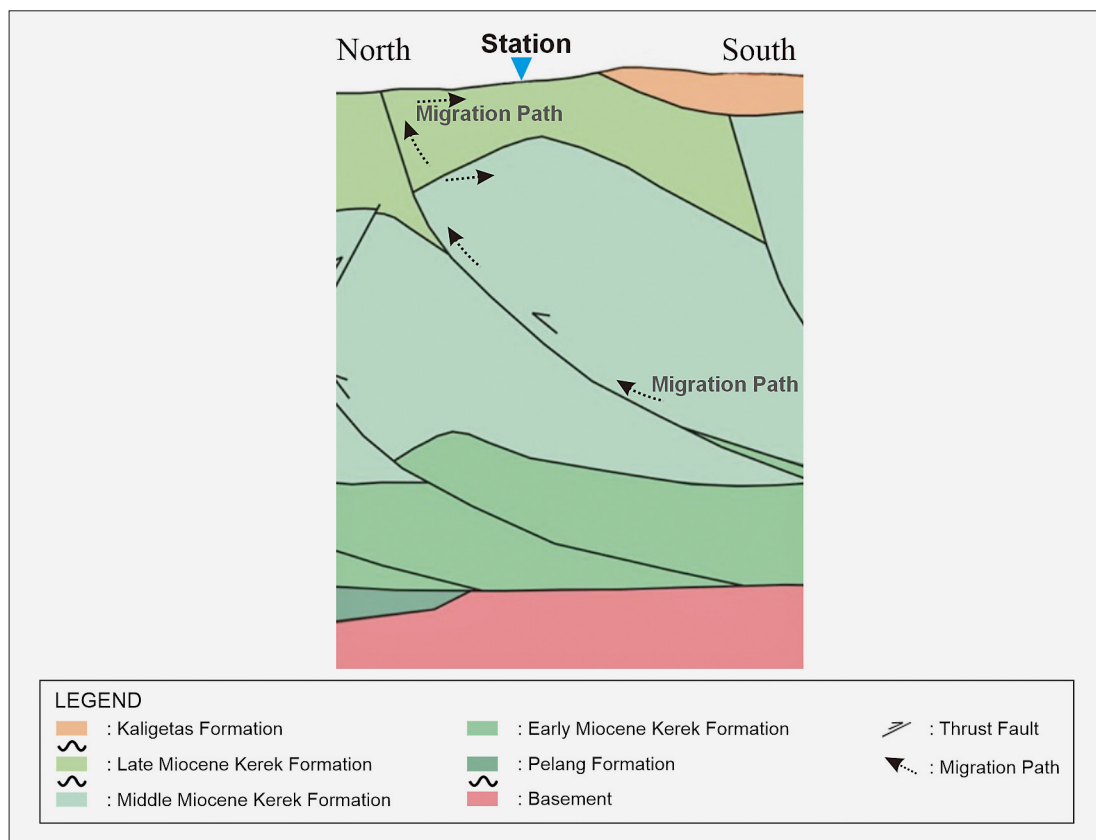**Figure 11.** Dip and azimuth calculation result for each station

Figure 12. The conceptual trap and recent hydrocarbon migration path around the research area
(modification from **Adha, 2019**)

In this equation, *H(f)* represents spectral amplitude of the horizontal component computed by taking the quadratic mean of the spectral amplitudes from both the east-west component (H_{EW}) and the north-south component (H_{NS}).

The VHSR is then calculated as the ratio of the vertical component's spectral amplitude to the horizontal component using the following **Equation 4**:

$$\text{VHSR}(f) = \frac{V(f)}{H(f)} \tag{4}$$

where *V(f)* refers to the spectral amplitude of the vertical component. **Priyono et al. (2023)** calculated the VHSR to be around 0.76-1.51 around the well. Meanwhile, **Saenger et al. (2009)** calculated a VHSR of 20-500 in production wells.

3. Results

Three-component waveform data record all seismic events. Not only background noise, but also all activity on the surface is recorded. Furthermore, by combining

the time window and bandpass filter, waveform data is selected to obtain the proper signal to analyse LFPS. **Figure 10** show the data selection and filter results for each station. Based on **Figure 10a**, the data at Station 1 responds to significant surface activity disturbances. This condition is due to the location of Station 1 around the well, which is right next to the highway. Therefore, the time window used at this station is the most at the data selection stage.

3.1.1. Polarization

The trap is a deformed rock bounded by a thrust fault (see **Figure 3**). The acquisition area is located around that fault that controls hydrocarbon migration. Fluid flow in recent hydrocarbon migration can provide induced seismicity. Therefore, conducting a polarity analysis to describe the seismic propagation that results from this phenomenon is necessary. The average dip using waveform data of five stations is 0.68^0 (see **Figure 11**), which means that the hydrocarbon flows horizontally. According to the trap style, the hydrocarbon flows horizontally in an anticline ridge near the surface. Another possibility is that the hydrocarbon flow comes from the northern fault bound to the trap. The second possibility is more acceptable because the average azimuth is -0.43^0 relative to the north.

4. Discussion

Seismic energy from natural sources typically propagates as body waves or surface waves. When those waves traverse hydrocarbon-bearing rocks, their behaviour differs distinctly from those in tight or water-saturated rocks. Additionally, flowing fluids can generate seismic waves propagating through the subsurface. We can see **Table 1** that shows the average porosity in specific depth interval. In order to discuss fluid flow, we must discuss the rock pore at the potential target. This data was obtained from Well K, which has a similar structural continuity. The depth range in the data is very shallow at 255-261 meters. The total porosity in this interval is 0.27. This porosity is taken only in the intercalated limestone of the Kerek Formation. With such good porosity, the mechanism by which hydrocarbons seep to the surface is an unanswered question in this study. Given the reasonably thick claystone in the Kerek Formation of the Late Miocene age, two possibilities are a seal damaged by deformation or a leaking fault that could become a hydrocarbon flow path.

Considering the above phenomena, this study aims to synthesize the phenomena recorded by seismometers related to hydrocarbon flow. This study aims to capture such responses using a seismometer, expecting anomalies to be detected within the 1-4 Hz frequency range that indicates the presence of hydrocarbon flow. **Figure 13** shows the PSD and VHSR results. This figure illus-

Table 1: The total porosity of Well K

	TVDSS (m)	PHI_{avg}
Top	255	0.27
Bottom	261	

trates the PSD anomaly is presence in low frequency range. That anomaly can be found in each station. In addition, the pick value of vertical-to-horizontal can be detected in that frequency range.

Station 1 is located near a well and adjacent to a roadway, requiring significant windowing of the acquired data to isolate representative signals. A notable anomaly in the low-frequency range of the Power Spectral Density (PSD) response suggests a correlation with hydrocarbons escaping from the well, with a PSD-IZ value of 0.866 and a VHRS of 0.684.

Station 2 is located at an oil seep emerging from a fracture in exposed bedrock near a river. Although the river was experiencing a minor flow at the time, the PSD anomaly is noticeable, though some contamination from the river cannot be entirely ruled out. However, the previous filtering steps should have minimized such effects. The PSD-IZ at this location is 0.33, and the VHRS is 0.78.

The PSD anomaly is pronounced at Station 3, near a well that releases oil and a small amount of gas. This agreeable response to the low-frequency anomaly is more significant than the surrounding stations, with a PSD-IZ value of 4.878 and a VHRS of 0.819.

Similarly, Station 4 is located near another oil well. In addition, this well released more gas than the previous wells. The PSD-IZ value here is 1.226, and the VHRS is 0.537.

Station 5 is located in an area without visible oil seepage but along the same structural features. This measurement was taken to determine if a similar response could be detected despite the absence of surface oil. PSD analysis shows the anomaly in the low-frequency range, and the PSD-IZ at this station is 3.625, and the VHSR is 1.324.

According to the above analysis, we can conclude that the behaviour of oil presence indicates a VHSR of more than 0.6. This behaviour differs from the presence of oil, which has a higher gas content (VHSR of less than 0.6).

Figure 12 is the conceptual model that explains the recent hydrocarbon migration. The hydrocarbon probably migrates along the fault. On the surface, we can find the Late Miocene Kerek Formation, which consists of claystone intercalated with limestone. The claystone characteristic is sealing. However, the existence of limestone in this formation may have increased the brittleness of the rock, causing open fractures. This fact can be found in the location of Station 2, where the opened fracture still emits oil seepage. The intercalated limestone probably allows the hydrocarbon to flow horizon-
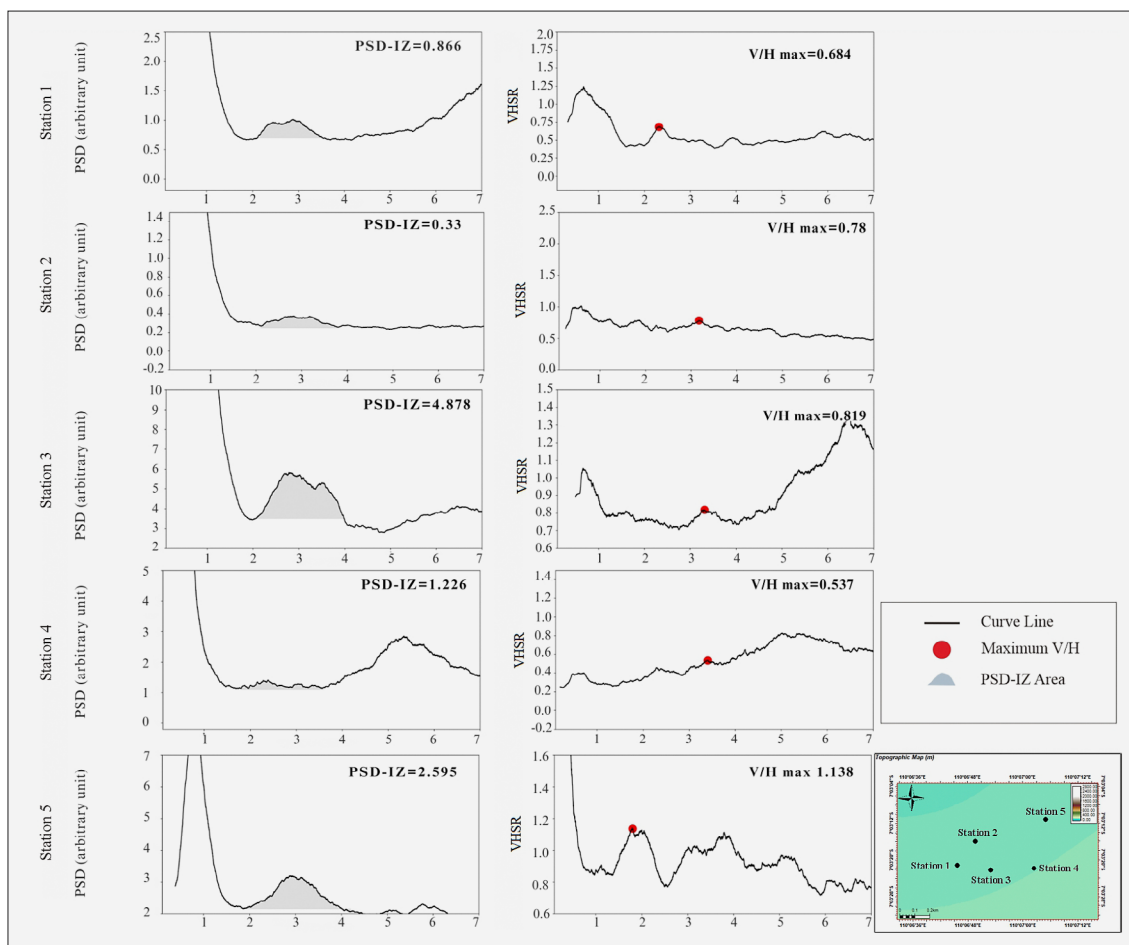
Figure 13. Power spectral density of vertical component and vertical-to-horizontal spectral ratio, indicating an anomaly in the frequency range 1.5-4 Hz in the Cipluk area.

tally. It is relevant to the results of the polarity analysis, which shows an average dip response of 0.68^0 from the north direction (0.43^0NNE).

5. Conclusions

LFPS research conducted in the Kendal subbasin area shows a correlation between the hydrocarbon presence at the well site and the oil seep site to spectral analysis. The PSD anomaly response in the low-frequency range and its PSD-IZ value have been shown. In addition, the results are reinforced by the peak value of VHSR in that frequency range. The results of this analysis can be used as DHI and strengthen/complement the analysis of the presence of hydrocarbons if other geophysical data are available.

Acknowledgement

6. References

Adha, I. (2019): Palinspastic Reconstruction of the Geological Structure of the Kali Lutut Area and Its Surroundings, Kendal-Temanggung, Central Java [Thesis], Institut Teknologi Bandung, Bandung.

Adha, I. and Sapiie, B. (2019): Rekonstruksi Struktur Geologi Kali Lutut dan Sekitarnya, Temanggung, Jawa Tengah, Jurnal Geosains dan Teknologi, 2 (2), 61-68.

Adha, I. (2021): Karakteristik Batuan Formasi Kerek Sebagai Reservoir di Lapangan Cipluk Kendal, Petrogas: Journal of Energy and Technology, 3 (2), 39-50.

Audithia W., Awari S., and Wiyono J. (2016): New Considerations for Petroleum System Implications of The Late Miocene Reservoir in The North Serayu Basin, Central Java, Fortieth Annual Convention and Exhibition, Indonesia.

Davis, J. C. (2006): Statistics and Data Analysis in Geology, 3nd ed. John Wiley and Sons, Knowledge as value: Clarification of zonation procedure (pp 646). New York, United State of America.

Flood, R.P., Orford, J.D., McKinley, J.M. and Roberson, S. (2015): Effective grain size distribution analysis for interpretation of tidal–deltaic facies: West Bengal Sundarbans, 318(2015), 58-74. http://dx.doi.org/10.1016/j.sedgeo.2014.12.007

Haris, A., Riyanto, A., Syahputra, R., Gunawan, A., Panguriseng, M. J., Nuratmaja, S., and Adriansyah. (2019): Integrating a microtremor survey and time reverse modeling over a hydrocarbon reservoir: A case study of Majalengka field, West Java Basin, Indonesia. Journal of Geophysics and Engineering, 16(1), 16–29. https://doi.org/10.1093/jge/gxy002

Jamal, J., Sanjaya, I., Saputro, D.H., and Suteja, A. (2024). Geological Structures in The Formation of The Kendal Plains: Insights from Remote Sensing Imagery. Journal of Geology and Mineral Resources, 25(4), 217-223. http://dx.doi.org/10.33332/jgsm.geologi.v25i4.827

Jolliffe, I.T. (2002): Principal Component Analysis, 2nd ed. New York, United State of America: Springer.

Koulakov, I., Bohm, M., Asch, G., Lühr, B., Manzanares, A., Brotopuspito, K.S., Fauzi, P., Purbawinata, M.A., Puspito, N.T., Ratdomopurbo, A., Kopp, H., Rabbel, W., and Shevkunova, E. (2007). P and S velocity structure of the crust and the upper mantle beneath central Java from local tomography inversion. Journal of Geophysical Research, 112. doi:10.1029/2006JB004712

Nurhandoko, B. E. B., Triyoso, K., Hadi, M. R. A., Rizal, I., Widarto, D. S., and Nurhasan. (2020): Miocene-Aged Aquifer Characterization in the Geological Complex of the Kendeng Thrust Fault Zone Using Rock Physics and Resistivity Tomography. Jurnal Geofisika, 18(2), 53-59.

Priyono, A., Ry, R.V., Nugraha, A.D., Lesmana, A., Prabowo, B.S., Husni, Y.M., Ardianto, A., Witarsa, N., and Sutan, B.I. (2023): On the use of Low-Frequency Passive Seismic as a Direct Hydrocarbon Indicator: A Case Study at Banyubang Oil Field, Indonesia. De Gruyter.

Rohaman, M., Winardhi, I.S., and Rizkianto, Y. (2022): The Application of Support Vector Machine to Estimate Synthetic Shear Sonic Log. Jurnal Ilmiah Magister Teknik Geologi.

Saenger, E.H., Schmalholz, S.M., Lambert, M.A., Nguyen, T.T., Torres, A., Metzger, S., Habiger, R.M., Muller, T., Rentsch, S., and Hernandez, E.M. (2009): A Passive Seismic Survey Over a Gas Field: Analysis of Low-Frequency Anomalies. Geophysics, 74(2), pp. 40.

Sribudiyani, Muchsin, N., Ryacudu, R., Kunto, T., Astono, P., Prasetya, I., Sapiie, B., Asikin, S., Harsolumakso, A.H., and Yulianto, I. (2003): The Collision of the East Java Microplate and Its Implication for Hydrocarbon Occurrence in the East Java Basin. Proceeding of the 29th Annual Convention. Jakarta, Indonesia, p. 335-346.

Sukardi, and Budhistrisna, T. (1992): Geological Map of Salatiga, Java. Geological Research and Development Center, Bandung.

Thanden, R.E., Sumardiredja, H., Richards, P.W., Sutisna, K., and Amin, T.C. (1996): Geological Map of Magelang and Semarang, Central Java. Geological Research and Development Center, Bandung.

Yang, Y., Zheng, G., Wang, Z., Chang, T., and Cui, H.-L. (2020): Seismic observation and analysis based on three-component fiber optic seismometer. IEEE Access, 8, 22916–22924. https://doi.org/10.1109/ACCESS.2019.2961963.

SAŽETAK

Analiza rezultata niskofrekventnih pasivnih seizmičkih istraživanja u svrhu karakterizacije prisutnosti ugljikovodika u subbazenu Kendal

Ovaj rad obuhvaća istraživanje karakteristika prisustva ugljikovodika u subbazenu Kendal, središnja Java, na temelju tehnika niskofrekventne pasivne seizmike (engl. *low-frequency passive seismic*, LFPS) kao izravnih indikatora ugljikovodika. Podatci o oblicima seizmičkih valova prikupljeni su 2024. godine putem pet postavljenih stanica, uključujući područja u blizini naftnih bušotina, prirodne izdanke nafte i zone u kojima nije bilo prirodnih izdanaka nafte, kako bi se procijenila prisutnost ugljikovodika zarobljenih unutar antiklinala omeđenih rasjedima. Na području istraživanja reverzni rasjedi s blagim nagibom znatno utječu na formaciju Kerek stvarajući strukturne nabore koji su potencijalne zamke ugljikovodika. U analizi toga potencijalnog sustava zamki oblici valova obrađuju se nakon određenoga vremenskog razdoblja i filtriranja prolaska kroj proslojke kako bi se poboljšala jasnoća signala i izdvojili relevantni seizmički odgovori. Ovo istraživanje identificiralo je znatne anomalije gustoće spektralne snage (engl. *power spectral density*, PSD) unutar frekvencijskoga raspona od 1 do 4 Hz, što je u skladu s anomalijama uočenim u podatcima o vertikalno-horizontalnome spektralnom omjeru (engl. *vertical-to-horizontal spectral ratio*, VHSR). Učestala pojava ovih anomalija u PSD i VHSR podatcima naglašava potencijal LFPS-a kao pouzdanoga alata za otkrivanje prisutnosti ugljikovodika u geološki složenim regijama kao što je subbazen Kendal. Također je provedena i analiza polariteta, iz koje proizlazi da je prosječni azimut 0,430 S-SI, s prosječnim padom od 0,680. Ti rezultati upućuju na dotok ugljikovodika od graničnoga rasjeda na sjeveru do bušotine. Ovom je metodom moguće dopuniti analize koje se temelje na drugim geofizičkim metodama, kako bi se pronašla nova nalazišta ugljikovodika.

Ključne riječi:
pasivna seizmika, niska frekvencija, spektralno, vertikalno-horizontalni spektralni omjer, gustoća spektralne snage

Author's contribution

Maman Rohaman (M.T., Geophysical Engineering with expertise in Seismic Exploration) performed the data acquisition, provided the LFPS data analysis, LFPS data interpretation, and composed the original draft and editing. **Alfathony Krisnabudhi** (M.T., Geological Engineering with expertise in Structural Geology and Petroleum Exploration) performed the field work, provided fault interpretation using gravity anomaly, and petroleum conceptualization. **Hasan Tri Atmojo** (M.T., Geological Engineering with expertise in Engineering Geology) performed the field work, provided data acquisition, and image enhancement. **Ikhwannur Adha** (M.T., Geological Engineering with expertise in Structural Geology and Tectonic) provided interpretation of regional stratigraphy and geological structures, fault interpretation, and petroleum conceptualization.
All authors have read and agreed to the published version of the manuscript.